

Streamwise and doubly-localised periodic orbits in plane Poiseuille flow

STEFAN ZAMMERT¹ † AND BRUNO ECKHARDT^{1,2}

¹ Fachbereich Physik, Philipps-Universität Marburg, Renthof 6, D-35032 Marburg, Germany

² J.M. Burgerscentrum, Delft University of Technology, Mekelweg 2, 2628 CD Delft, The Netherlands

(Received 3 December 2024)

We study localised exact coherent structures in plane Poiseuille flow that are relative periodic orbits. They are obtained from extended states in smaller, periodically continued domains, by increasing the length to obtain streamwise localization and then by increasing the width to achieve spanwise localisation. The states maintain the travelling wave structure of the extended states, which is then modulated by a localised envelope on larger scales. In streamwise direction, the envelope shows exponential localization, with different exponents on the upstream and downstream side. The upstream exponent increases linearly with Reynolds number Re , but the downstream exponent is essentially independent of Re . In the spanwise direction the decay is compatible with a power-law localisation. As the width increases the localised state undergoes further bifurcations which add additional unstable directions, so that the edge state in the system becomes chaotic.

1. Introduction

The study of coherent structures in small periodic domains, often referred to as 'minimal flow units', has provided considerable insight into the phase space structure and the transition dynamics of shear flows without linear instabilities of the laminar state, such as pipe flow or plane Couette flow and various boundary layers (e.g. Kreilos & Eckhardt (2012) and references therein). For an understanding of the fascinating spatio-temporal dynamics in the transition region, where intriguing patterns of alternating laminar and turbulent dynamics (Barkley & Tuckerman 2005; Duguet *et al.* 2010) and a complicated evolution that has been linked to directed percolation (Manneville 2009; Moxey & Barkley 2010; Avila *et al.* 2011) can be observed, it is necessary to investigate spatially extended domains and localised states. The interest in localised solutions arises also from the possibility to use them as building blocks for more complicated spatial patterns, such as the turbulent spots observed in plane Couette or plane Poiseuille flow in various experimental (e.g. Carlson *et al.* 1982; Dauchot & Daviaud 1995; Hegseth 1996; Lemoult *et al.* 2013) and numerical (e.g. Henningson *et al.* 1987; Lundbladh & Johansson 1991; Schumacher & Eckhardt 2001) studies.

The spatially extended exact coherent structures arise in the form of stationary states without any time-dependence, travelling waves where a pattern moves downstream with a fixed speed, or relative periodic orbits that return to the initial pattern except for a displacement (Nagata 1990, 1997; Ehrenstein *et al.* 1991; Schmiegél 1999; Wang *et al.* 2007; Gibson *et al.* 2009). Spanwise localised exact states have been identified by Schneider *et al.* (2010a,b), Gibson & Brand (2014) and Zammert & Eckhardt (2014) for plane

† Email address for correspondence: stefan.zammert@physik.uni-marburg.de

Couette and plane Poiseuille flow. Streamwise localised exact solutions have been described for the case of 2D plane Poiseuille flow (Price *et al.* 1993) and for pipe flow (Avila *et al.* 2013; Chantry *et al.* 2014). Spanwise localised states in plane Poiseuille flow show a complicated temporal dynamics (Zammert & Eckhardt 2014) that has also been documented for the asymptotic suction boundary layer by Khapko *et al.* (2013, 2014). A state in plane Couette flow that is localised in both spanwise and streamwise direction has been identified recently by Brand & Gibson (2014).

In this paper we present coherent structures for plane Poiseuille flow that are localised in the streamwise direction and in streamwise and spanwise direction. We find them using the method of edge tracking (Skufca *et al.* 2006) in small periodic domains, and then track them first to longer and then also to wider domains. We begin with a discussion of the extended states in narrow domains in section 2, followed by studies of streamwise localised states in section 3 and spanwise and streamwise localised structures in section 4. Conclusions are given in section 5.

2. The edge state in short domains - A traveling wave

We study the incompressible plane Poiseuille flow (PPF), the pressure driven flow between two infinitely extended parallel plates. With the x -axis along the flow direction, the plates are parallel to the x - z plane at $y = \pm h$. The Reynolds number is based on h , the laminar centre-line velocity U_0 and the kinematic viscosity ν , so that $Re = U_0 h / \nu$ and the laminar non-dimensional profile becomes $U(y) = (1 - y^2)$. In all our simulations constant mass-flux is imposed. The velocity fields used in the following are the deviations from the laminar profile, denoted $\mathbf{u} = (u, v, w)$, where u , v , and w are the streamwise, wall-normal and spanwise velocity components, respectively.

The numerical simulations are based on the spectral code *channelflow*, developed and maintained by Gibson (2012). The package provides a Newton-method (Viswanath 2007) for searching exact solutions as well as tools for continuation and stability analysis. We adapted the *channelflow*-code to work with parallel FFTW (OpenMP) and replaced the *Octave*-library used for the linear algebra routines in the Newton-method and the eigenvalue calculations by the *Eigen*-package (Guennebaud, Jacon & Others 2010). The method of edge tracking algorithm is described, e.g. by Toh & Itano (2003), Skufca *et al.* (2006), Schneider *et al.* (2008) and Dijkstra *et al.* (2014).

We started off with edge tracking from a random initial condition in a small periodic domain with streamwise length L_x of 2π and spanwise width L_z of 2π with a numerical resolution of $N_x \times N_y \times N_z = 32 \times 65 \times 48$ and a Reynolds number of 1400. We checked our resolution by comparing to a higher one of $N_x \times N_y \times N_z = 80 \times 97 \times 112$. For this Re plane Poiseuille flow shows persistent turbulence although it is far below the critical Reynolds number of 5772 (Orszag 1971) that follows from linear stability theory for this geometry. Edge tracking usually converges quickly to one travelling wave, referred to as TW_E in the following. This state has two symmetries, a mirror symmetry with respect to the mid-plane, and a shift and reflect symmetry in the spanwise direction,

$$s_y : [u, v, w](x, y, z) = [u, -v, w](x, -y, z), \quad (2.1)$$

$$s_z \tau_x : [u, v, w](x, y, z) = [u, v, -w](x + L_x/2, y, -z). \quad (2.2)$$

The state is dominated by a strong low speed streak in the midplane and pairs of vortices at the top and bottom plate. It is qualitatively different from the travelling waves in PPF described by Waleffe (1998, 2003) and Nagata & Deguchi (2013), but it has the same symmetry as TW1-1 from Gibson & Brand (2014).

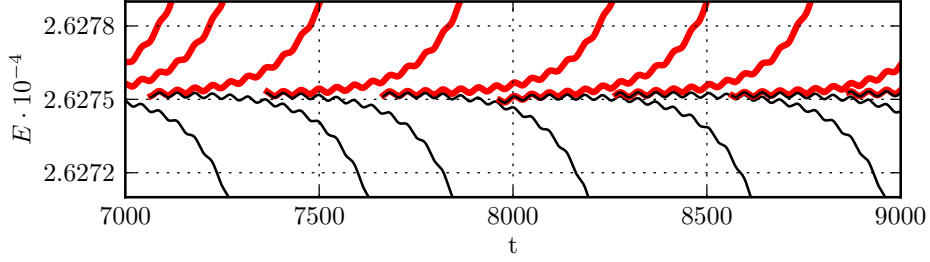


FIGURE 1. Edge tracking in a computational domain of length $L_x = 32\pi$ and width $L_z = 2\pi$ for $Re = 1400$. Shown are the energies of trajectories that turn turbulent (red thick) and laminar (black thin), respectively. The edge state bracketed by these trajectories oscillates periodically in energy.

Stability analysis of the travelling wave in the full space without any symmetry restriction shows that it has one unstable eigenvalue for $510 < Re < 5850$ so that its stable manifold is of co-dimension one. A stability analysis of this periodic state in longer domains shows that already for $L_x = 4\pi$ the state has an additional pair of unstable complex conjugated eigenvalues for $Re < 1785$. Further doubling of the domain size adds more unstable directions, so that, e.g., for $L_x = 8\pi$ and $Re = 1400$ the wave has 5 unstable eigenvalues. The long-wavelength instabilities in the larger domains are precursors to localisation in spanwise (Melnikov *et al.* 2014) and streamwise direction (Chantry *et al.* 2014).

3. Streamwise localised periodic orbits in long domains

In a longer domain of length 32π but with the same width of 2π and at Reynolds number $Re = 1400$, edge tracking converges to a state that at first glance looks like a state of constant energy,

$$E(\mathbf{u}) = \frac{1}{2L_x L_z} \int \mathbf{u}^2 dx dy dz. \quad (3.1)$$

However, closer inspection of the timetrace in figure 1 reveals that it is not constant but shows a regular oscillation with an amplitude of order 10^{-8} . This oscillation is not a numerical artefact but reflects properties of the edge state, as we now show.

Although the initial velocity field is spatially non-localised, the flow state obtained by edge tracking is localised in streamwise direction. Using this state as an initial condition in a Newton-method, we quickly converge to a streamwise localised relative periodic orbit, referred to as PO_E in the following. For further study we transfer the state to a computational domain of length 64π , which is possible because of its streamwise localisation. We use a resolution of $768 \times 65 \times 48$ and check our results with a higher spanwise resolution of $N_z = 80$. The streamwise and the spanwise velocity components in the mid-plane are shown in figure 2. Cross-sections for $Re = 1400$ for different streamwise positions are shown in figure 3 (a) - (d) and the streamwise averaged velocity is shown in (e). The images reveal that the orbit has a mirror symmetry (s_y) but no $s_z \tau_x$ -symmetry and is dominated by a strong narrow low-speed streak and a weak and extended high-speed streak. It is therefore very similar to the travelling wave TW_E . In particular, the streamwise averaged flow for TW_E is close to the one shown in figure 3 (e).

The complex spatial propagation pattern of the wave can be seen figure 4 where the spanwise velocity in the midplane at $z = 0$ is plotted versus time for $Re = 1410$. The

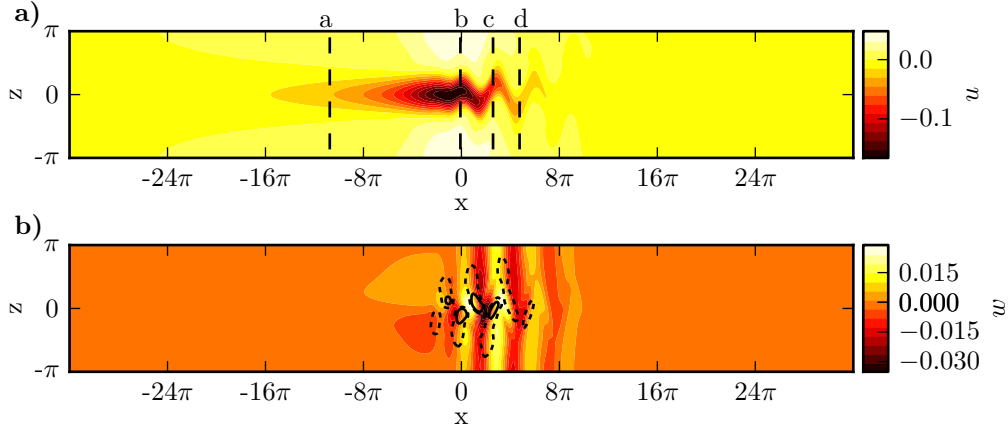


FIGURE 2. Velocities in the mid-plane for the edge state PO_E at $Re = 1400$. Shown are the (a) streamwise and (b) spanwise velocities. The black lines in (a) mark the positions of the spanwise wall-normal cross sections in 3 (a)-(d). The solid and dashed lines in (b) are iso-contours of the Q-vortex criterion (Jeong & Hussain 1995) at levels of 0.001 and 0.0001 , respectively. The direction of the flow is from left to right.

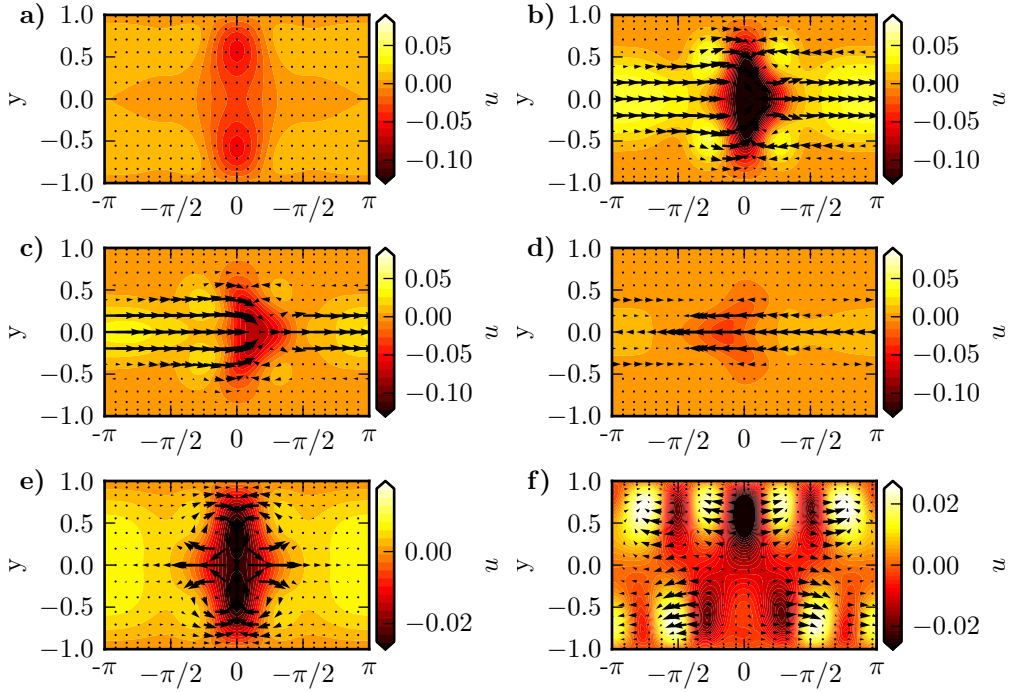


FIGURE 3. (a) - (d) Cross sections of the edge state PO_E at $Re = 1400$ at the streamwise positions indicated in figure 2(b). The in-plane components of the velocity are indicated by arrows and the streamwise component is colour coded. (e) and (f) show the streamwise-averages of PO_E at $Re = 1400$ and of the orbit that bifurcates from it, PO_{asy} , at $Re = 1625$, respectively.

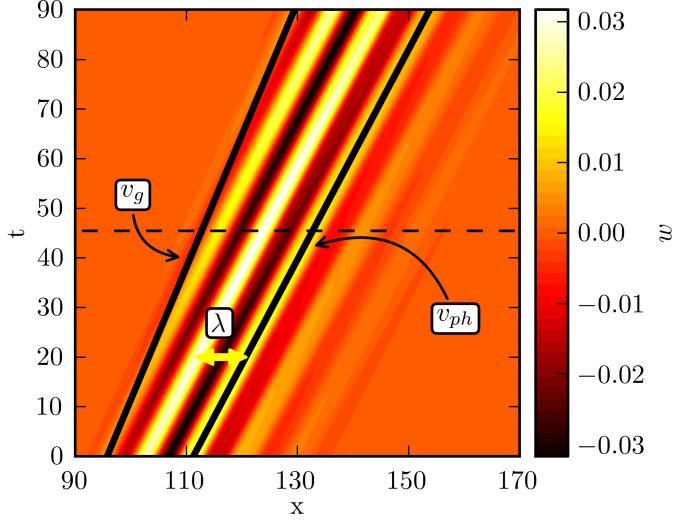


FIGURE 4. Space-time-display of the spanwise velocity of the periodic orbit PO_E in the mid-plane $y = 0$ at $z = 0$ for $Re = 1400$. The solid black lines indicate the group velocity v_g and the phase velocity v_{ph} for one of the maxima. The wavelength λ of the internal modulations varies along the state. The dashed black line marks one period T in energy.

total energy of the state is periodic with a period $T = 45.402$, but the state needs twice this time to return in shape, up to a downstream shift. After a time T it returns up to a symmetry operation $s_z : [u, v, w](x, y, z) = [u, v, -w](x, y, -z)$ and a downstream shift that is half the one after $2T$. The figure clearly shows a group velocity v_g for the envelope of the state, and a phase velocity v_{ph} for the underlying structures. The group velocity v_g can be calculated by dividing the distance travelled over two periods by $2T$. For $Re = 1400$ one obtains $v_g = 0.8753$, indicated by the line at the upstream end of the state in figure 4. The structures underneath the envelope move with a different velocity v_{ph} , which can be read off from the slope of the maxima. However, the wavelength λ of the spanwise modulations varies slightly with position and is slightly larger at the front than in the centre and towards the end of the state. Therefore, also the velocity of each maximum varies slightly, so that the phase velocity depends on the position within the state.

Using a continuation method (see e.g. Dijkstra *et al.* 2014) it is easy to track the state in Re . It turns out that the periodic orbit exists down to $Re \approx 1038$, where it is created in a saddle node bifurcation. Furthermore, it is also possible to identify the upper branch of the periodic orbit. This upper branch is also localised and has multiple unstable directions.

A stability analysis of the lower branch state shows that for $Re > 1100$ it has one unstable direction. Therefore, for these Reynolds numbers the state is an edge state whose stable manifold can separate the state space into two parts. For lower values of Re the periodic orbit has more than one unstable direction. The bifurcation near $Re \approx 1100$ is a Sacker-Neimark bifurcation (Kuznetsov 1998) that breaks the s_y symmetry. This bifurcation is followed by further bifurcations resulting in eight unstable directions for the lower branch. One of the bifurcations of the lower branch is a pitchfork bifurcation that breaks the s_y symmetry and creates an asymmetric periodic orbit (PO_{asy}). The image of the state in figure 3 (f) shows that its internal dynamics is more complex than

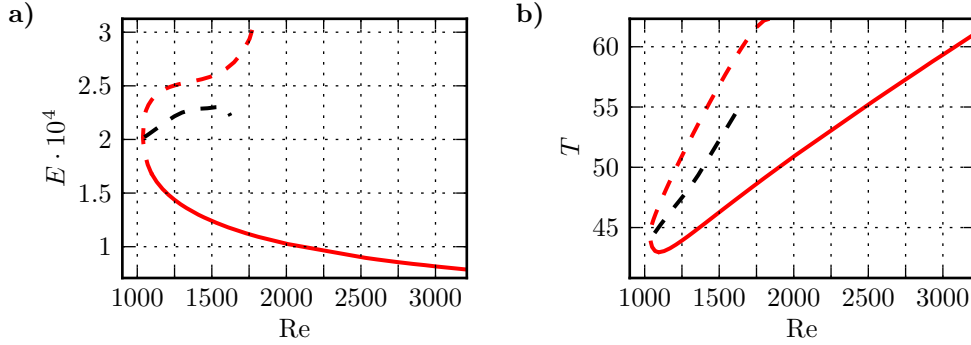


FIGURE 5. Bifurcation diagram for the coherent structures. (a) Minimum energy of the localised periodic orbit PO_E (red) and the asymmetric orbit PO_{asy} (black) vs Re . In both cases the minimum in energy over the period T is shown. The stability of the orbit is indicated by the linetype, solid for a single unstable direction, and dashed for more than one. (b) Variation of the periods in energy with Re .

that of PO_E . The bifurcations and some properties of the states are summarised in figure 5.

Information about the localization properties can be extracted from the streamwise variation of the energy density of the deviation from the laminar flow,

$$E_{\perp}(x) = \frac{1}{2L_z} \int_0^{L_z} \int_{-1}^1 \mathbf{u}^2 dydz, \quad (3.2)$$

and the density of the cross-flow energy

$$E_{\perp,c}(x) = \frac{1}{2L_z} \int_0^{L_z} \int_{-1}^1 v^2 + w^2 dydz. \quad (3.3)$$

The energy densities for the periodic orbit at $Re = 2010$ (at times of minimal energy) are shown in figure 6(a). One can identify a small region with relatively high cross-flow energy at the front of the state. In this region the cross flow draws energy from the laminar profile and transfers it into streamwise velocity, which then drives streaks and causes a steep increase of the total energy density at the front of the state. The energy in the streamwise components has its maximum at a position in the tail where the cross-flow energy is already very low again. In the absence of cross-flow motion the streaks are damped by viscosity only, which results in the long tail of the state.

Based on the energy density $E_{\perp}(x)$ one can introduce two characteristic length scales for PO_E , associated with the extension in the downstream and upstream direction. Starting from the maximum in energy, one can determine the distances to the locations where the energy density has dropped to half its maximum. They are denoted l_t and l_h for the upstream (tail) and downstream (head) sides, respectively, and are shown in figure 6(b). On the downstream side, the energy drops off quickly, on a length scale that varies very little with Re . On the upstream side, the energy drops off more slowly, on a length scale that increases linearly with Re . The origin of this scaling is the viscous decay of the streaks on a time scale proportional to Re , which then is translated into a spatial scale proportional to Re by the essentially constant advection velocity. In the case of plane Couette flow, Brand & Gibson (2014) have been able to determine the slopes from a linear stability analysis that confirms this scaling. The case of plane Poiseuille flow is more complicated because the state is not stationary, and an analytical calculation of the decay rates has not been possible, yet.

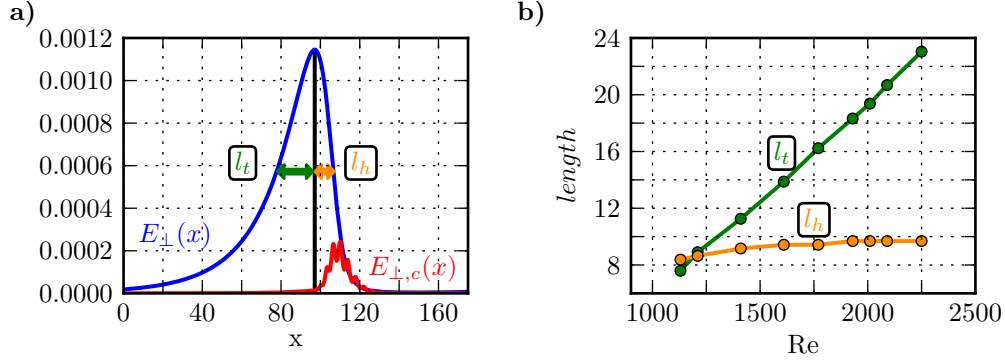


FIGURE 6. Energy profiles of the localised state. (a) Densities of total (red) and the cross flow (blue) energy for the periodic orbit at $Re = 2010$ along the flow direction, which is from left to right. The cross flow energy density is multiplied by a factor of 10. (b) Downstream l_h (orange) and upstream l_t (green) distances from the maximum to half the maximal values in energy.

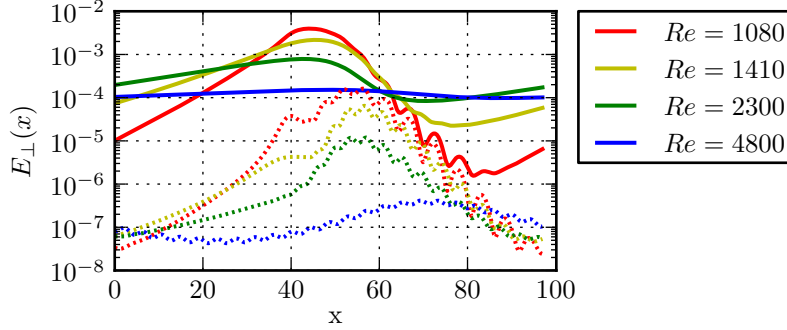


FIGURE 7. Profiles of PO_E for increasing Reynolds numbers. The solid lines show the total and the dashed lines the cross-flow energy densities. Consistent with the increase in l_d , the states become more and more delocalised with increasing Reynolds number, until they merge into a spatially extended state near $Re = 5385$. The streamwise length of the computational domain is 32π .

Although the structure becomes longer with increasing Re , the total energy and also the maximum of the energy density decrease with increasing Re (see figure 5). In finite domains the increasing length of the structures will then cause interferences between head and tail and a loss of localisation. For instance, continuation of PO_E to high Re in a box of length 32π shows that the orbit connects to the streamwise extended travelling wave TW_E at $Re \approx 5385$ with a wavelength of 2.66π . This is documented in figure 7 in a plot of the energy densities vs. Re . For low Re there is a pronounced maximum in the densities, but for increasing Re the differences decrease and finally at $Re \approx 5380$ the uniform energy density corresponding to the travelling wave is obtained. Turned the other way round, the localised state arises out of a streamwise long-wavelength instability of a travelling wave, very much as the long wavelength instabilities discussed in plane Couette flow (Melnikov *et al.* 2014) or in pipe flow (Chantry *et al.* 2014).

4. A streamwise and spanwise localised periodic orbit

The periodic orbits found in the domain with $L_z = 2\pi$ are localised in the streamwise direction. They show early signs of localisation in the spanwise direction in that the

energy density close to the strong low-speed streak is much higher than in the region of the high-speed streak. To obtain periodic orbits that are also localised in the spanwise direction we continue the periodic orbit in box width. For the continuation in L_z we fix $Re = 2180$ and a length of 64π . As a measure of the state we consider the energy density obtained by averaging over the streamwise and normal directions,

$$E_{\parallel}(z) = \frac{1}{2L_x} \int_0^{L_x} \int_{-1}^1 \mathbf{u}^2 \, dx dy. \quad (4.1)$$

This partially averaged energy density depends on the spanwise coordinate only, and is shown in figure 8(a) for various widths L_z . The maximum at $z = 0$ corresponds to the position of the low-speed streak. For $L_z = 2\pi$ the second smaller maximum is the position of the weak high speed streak. Slightly above $L_z = 2\pi$ the lower maximum splits into two. For $L_z > 5\pi$ the energy density has a very low value over most of the domain, indicating a spanwise localised flow structure. The largest value of L_z which we studied is 72π . For this domain we use a resolution of $N_x \times N_y \times N_z = 384 \times 49 \times 1728$. The doubly-localised solution in this domain keeps the s_y symmetry of the state that is localised in streamwise direction only. The period T of the orbit is 53.578. After this time the state returns in shape up to a downstream shift and the symmetry operation s_z . The group-speed of the orbit is $v_g = 0.8803$.

The logarithmic scale in figure 8(a) shows that $E_{\parallel}(z)$ does not drop off exponentially. The integrated density increases with the length of the turbulent region, so that a much better measure is the maximum in velocities along x and y for a fixed spanwise position, i.e the ∞ -norm $\mathcal{L}^{\infty}(z) = \max_{x,y} |u(x, y, z)|$, here given for the streamwise component u (Brand & Gibson 2014). Its values for the streamwise and spanwise component are shown in figure 9(a). The decay of $\mathcal{L}^{\infty}(u)$ is slower than exponential while $\mathcal{L}^{\infty}(w)$ drops off even faster. The second part is hidden in $E_{\parallel}(z)$ because it is swamped by the higher values of the streamwise component. The behaviour near $z = L_z$ is clearly influenced by the boundary conditions: the streamwise component is symmetric under reflection at the boundary, whereas the spanwise component is antisymmetric and vanishes at the boundary. Taking this into account, the figure also shows fits to an algebraic decay with the correct symmetries: the agreement between the fit and the numerical data indicates that the velocity fields fall off like $1/z^2$.

In the streamwise direction, as documented in figure 9(b), the decay is exponential, as found for the partially localised states in section 3, with the same asymmetry in the decays in the upstream and downstream direction.

Images of the streamwise and the spanwise velocity fields in the midplane are shown in figure 10. The visualization of the spanwise velocity reveals a large-scale, quadrupolar-like flow field, where the centres of the left and the right pairs of lobes coincide with intensity maxima of $E_{\perp,c}(x)$. The quadrupolar shape of the spanwise velocity also exists away from the midplane, but becomes less distinct close to the walls. Given the observation of similar large scale quadrupole flows in turbulent spots in plane Couette (e.g. Schumacher & Eckhardt 2001; Lagha & Manneville 2007; Duguet & Schlatter 2013; Gibson & Brand 2014) and plane Poiseuille flow (Lemoult *et al.* 2013, 2014), one can anticipate that they appear for all structures that are localised in all directions.

We verified that we can trace the doubly localised solution in the domain with $L_x = 64\pi$ and $L_z = 72\pi$ also to lower and higher values of Re , but because applying the Newton-method to this large domain is computationally very expensive, we did not perform a complete continuation in Reynolds number.

A stability analysis of the localised state as a function of L_z at $Re = 2180$ shows that it has two unstable eigenvalues for $L_z \geq 6\pi$. Therefore, it is not an attracting

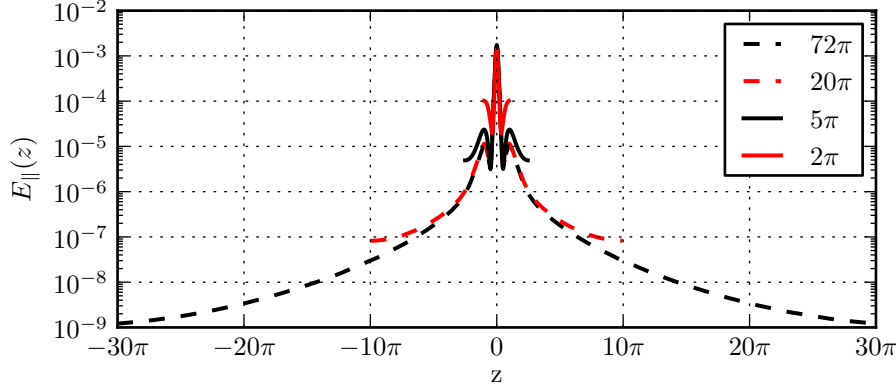


FIGURE 8. Spanwise profiles of the total energy of the localised states PO_E for various spanwise widths L_z .

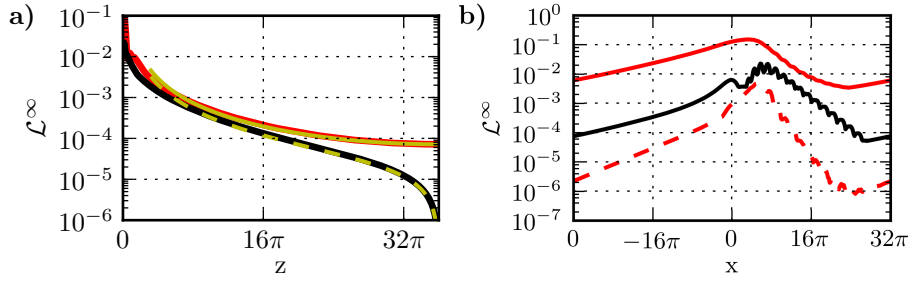


FIGURE 9. In (a) the \mathcal{L}^∞ -norm (maximum over y and x) of the streamwise u (solid red), the spanwise w (solid black) velocity component versus spanwise coordinate z are shown. The yellow lines show fits $A(z^2 + (L_z - z)^2)$ (solid) and $A(z^2 - (L_z - z)^2)$ (dashed). (b) shows the \mathcal{L}^∞ -norms (maximum over y and z) of the streamwise (solid red), spanwise (black) and wall-normal (dashed red) velocity component versus streamwise coordinate x .

state in the laminar-turbulent boundary. Edge tracking calculations starting from the disturbed localised periodic orbit do not result in a simple attractor. Instead, the time evolution of the state is chaotic, but it remains localised (Zammert & Eckhardt 2014b). This behaviour is similar to what has been seen in large plane Couette domains (Marinc *et al.* 2010; Schneider *et al.* 2010b; Duguet *et al.* 2009), long pipes (Mellibovsky *et al.* 2009), or wide domains in the asymptotic suction boundary layer (Khapko *et al.* 2014).

5. Conclusions and Outlook

We were able to identify a doubly localised periodic orbit in plane Poiseuille flow. The orbit was shown to bifurcate from a streamwise extended travelling wave. Together with the other current examples of long-wavelength instabilities (Melnikov *et al.* 2014; Chantry *et al.* 2014) we anticipate that many more localised states can be found in bifurcations of the myriad of spatially extended states that have been identified already (Schmiegel 1999; Gibson *et al.* 2009). Homotopies between plane Poiseuille flow and other flows, including plane Couette or the asymptotic suction boundary layer, can then reveal connections between these states (Waleffe 2003; Kreilos *et al.* 2013). More generally, the presence of localised states opens up the road to spatial delocalisation and the development of spatio-temporal patterns (see e.g. Barkley & Tuckerman 2005; Avila *et al.* 2011;

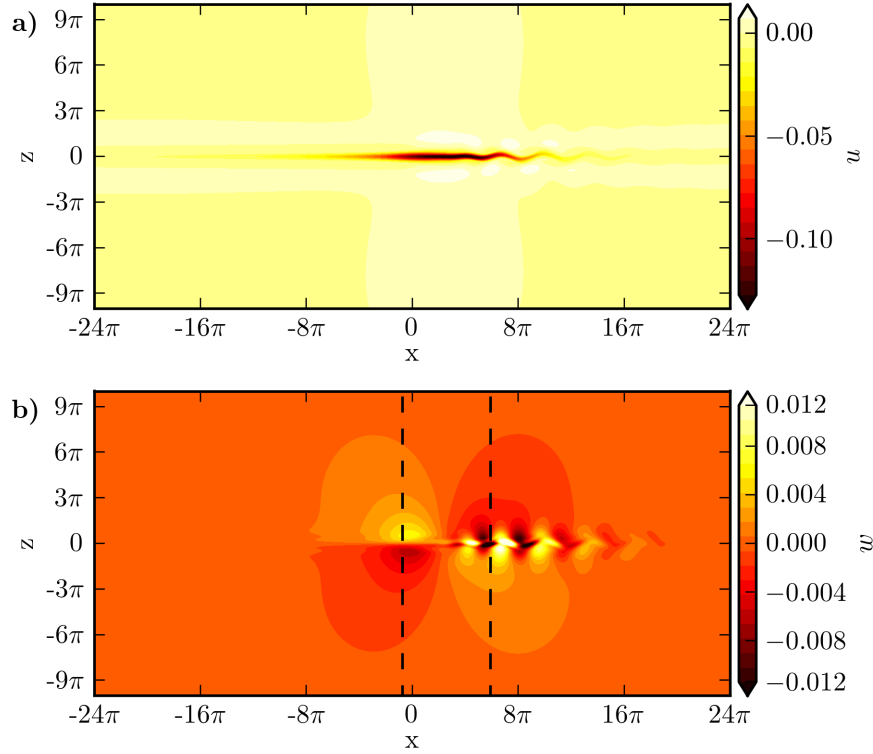


FIGURE 10. Streamwise (a) and spanwise (b) velocity in the mid-plane for the doubly-localised periodic orbit at $Re = 2180$ in a domain with $L_x = 64\pi$ and $L_z = 72\pi$. Only the part of the domain that contains the localised flow structure is shown. The dashed lines in (b) mark the downstream positions of the maxima in the energy density $E_{\perp,c}(x)$.

Tuckerman *et al.* 2014).

Acknowledgements We thank John Gibson for providing *channelflow* and stimulating exchanges on localization properties. We also thank Yohann Duguet and Tobias Kreilos for discussions. This work was supported by the Deutsche Forschungsgemeinschaft within FOR 1182.

REFERENCES

- AVILA, K., MOXEY, D., DE LOZAR, A., AVILA, M., BARKLEY, D. & HOF, B. 2011 The onset of turbulence in pipe flow. *Science* **333** (6039), 192–196.
- AVILA, M., MELLIBOVSKY, F., ROLAND, N. & HOF, B. 2013 Streamwise-localised solutions at the onset of turbulence in pipe flow. *Phys. Rev. Lett.* **110**, 224502.
- BARKLEY, D. & TUCKERMAN, L. 2005 Computational study of turbulent laminar patterns in Couette flow. *Phys. Rev. Lett.* **94**, 014502.
- BRAND, E. & GIBSON, J.F. 2014 A doubly-localised equilibrium solution of plane Couette flow. *J. Fluid Mech.* **750**, R1.
- CARLSON, D. R., WIDNALL, S. E. & PEETERS, M. F. 1982 A flow-visualization study of transition in plane Poiseuille flow. *J. Fluid Mech.* **121**, 487–505.
- CHANTRY, M., WILLIS, A. P. & KERSWELL, R. R. 2013 The genesis of streamwise-localised solutions from globally periodic travelling waves in pipe flow. *Phys. Rev. Lett.* **112**, 164501.

- DAUCHOT, O. & DAVIAUD, F. 1995 Finite amplitude perturbation and spots growth mechanism in plane Couette flow. *Phys. Fluids* **7**, 335.
- DIJKSTRA, H., *et al.* 2014 Numerical bifurcation methods and their application to fluid dynamics: Analysis beyond simulation. *Commun. Comput. Phys.* **15**, 1–45.
- DUGUET, Y. & SCHLATTER, P. 2013 Oblique laminar-turbulent interfaces in plane shear flows. *Phys. Rev. Lett.* **110**, 034502.
- DUGUET, Y., SCHLATTER, P. & HENNINGSON, D. S. 2009 Localised edge states in plane Couette flow. *Phys. Fluids* **21**, 111701.
- DUGUET, Y., SCHLATTER, P. & HENNINGSON, D. S. 2010 Formation of turbulent patterns near the onset of transition in plane Couette flow. *J. Fluid Mech.* **228**, 119–129.
- EHRENSTEIN, U. & KOCH, W. 1991 Three-dimensional wavelike equilibrium states in plane Poiseuille flow. *J. Fluid Mech.* **121**, 111–148.
- GIBSON, J. F. 2012 Channelflow: A spectral Navier-Stokes simulator in C++. *Tech. Rep.*. U. New Hampshire. www.channelflow.org.
- GIBSON, J. F. & BRAND, E. 2014 Spanwise-localised solutions of planar shear flows. *J. Fluid Mech.* **745**, 25–61.
- GIBSON, J. F., HALCROW, J. & CVITANOVIĆ, P. 2009 Equilibrium and travelling-wave solutions of plane Couette flow. *J. Fluid Mech.* **638**, 243–266.
- GUENNEBAUD, G., JACON, B. & OTHERS 2010 Eigen v3 <http://eigen.tuxfamily.org>.
- HEGSETH, J. 1996 Turbulent spots in plane Couette flow. *Phys. Rev. E* **54**, 4915–4923.
- HENNINGSON, D., SPALART, P. & KIM, J. 1987 Numerical simulations of turbulent spots in plane Poiseuille and boundary-layer flow. *Phys. Fluids* **30**, 2914.
- JEONG, J. & HUSSAIN, F. 1995 On the identification of a vortex. *J. Fluid Mech.* **285**, 69–94.
- KHAPKO, T., KREILOS, T., SCHLATTER, P., DUGUET, Y., ECKHARDT, B. & HENNINGSON, D. S. 2013 Localised edge states in the asymptotic suction boundary layer. *J. Fluid Mech.* **717**, R6.
- KHAPKO, T., DUGUET, Y., KREILOS, T., SCHLATTER, P., ECKHARDT, B. & HENNINGSON, D. S. 2014 Complexity of localised coherent structures in a boundary-layer flow. *Eur. Phys. J. E* **37**, 32.
- KREILOS, T. & ECKHARDT, B. 2012 Periodic orbits near onset of chaos in plane Couette flow. *Chaos* **22**, 047505.
- KREILOS, T., VEBLE, G., SCHNEIDER, T. M. & ECKHARDT, B. 2013 Edge states for the turbulence transition in the asymptotic suction boundary layer. *J. Fluid Mech.* **726**, 100–122.
- KUZNETSOV, Y. A. 1998 *Elements of applied bifurcation theory*. Springer Berlin / Heidelberg.
- LAGHA, M. & MANNEVILLE, P. 2007 Modeling of plane Couette flow. I. Large scale flow around turbulent spots. *Phys. Fluids* **19**, 094105.
- LEMOULT, G., AIDER, J.-L. & WESFREID, J. E. 2013a Turbulent spots in a channel: large-scale flow and self-sustainability. *J. Fluid Mech.* **731**, R1.
- LEMOULT, G., GUMOWSKI, K., AIDER, J.-L. & WESFREID, J. E. 2014 Turbulent spots in channel : an experimental study Large-scale flow, inner structure and low order model. *Eur. Phys. J. E* **37**, 25.
- LUNDBLADH, A. & JOHANSSON, A. V. 1991 Direct simulation of turbulent spots in plane Couette flow. *J. Fluid Mech.* **229**.
- MANNEVILLE, P. 2009 Spatiotemporal perspective on the decay of turbulence in wall-bounded flows. *Phys. Rev. E* **79**, 025301.
- MARINC, D., SCHNEIDER, T. M. & ECKHARDT, B. 2010 localised edge states for the transition to turbulence in shear flows. In *Seventh IUTAM Symp. Laminar-Turbulent Transit.* (ed. Philipp Schlatter & Dan S. Henningson), *IUTAM Bookseries*, vol. 18, pp. 253–258. Dordrecht: Springer Netherlands.
- MELLIBOVSKY, F., MESEGUER, A., SCHNEIDER, T. & ECKHARDT, B. 2009 Transition in localised Pipe Flow Turbulence. *Phys. Rev. Lett.* **103**, 054502.
- MELNIKOV, K., KREILOS, T. & ECKHARDT, B. 2014 Long wavelength instability of coherent structures in plane Couette flow. *Phys. Rev. E* **89**, 043088.
- MOXEY, D. & BARKLEY, D. 2010 Distinct large-scale turbulent-laminar states in transitional pipe flow. *Proc. Natl. Acad. Sci. U. S. A.* **107**, 8091–8096.
- NAGATA, M. 1990 Three-dimensional finite-amplitude solutions in plane Couette flow: bifurcation from infinity. *J. Fluid Mech.* **217**, 519–527.

- NAGATA, M. 1997 Three-dimensional traveling-wave solutions in plane Couette flow. *Phys. Rev. E* **55**, 2023–2025.
- NAGATA, M. & DEGUCHI, K. 2013 Mirror-symmetric exact coherent states in plane Poiseuille flow. *J. Fluid Mech* **735**, R4.
- ORSZAG, S. A. 1971 Accurate solution of the Orr–Sommerfeld stability equation. *J. Fluid Mech.* **50**, 689–703.
- PRICE, T., BRACHET, M. & POMEAU, Y. 1993 Numerical characterization of localised solutions in plane Poiseuille flow. *Phys. Fluids A Fluid Dyn.* **5**, 762.
- SCHMIEGEL, ARMIN 1999 Transition to turbulence in linearly stable shear flows. Phd thesis, Marburg.
- SCHNEIDER, T. M., GIBSON, J. F., LAGHA, M., DE LILLO, F. & ECKHARDT, B. 2008 Laminar-turbulent boundary in plane Couette flow. *Phys. Rev. E* **78**, 037301.
- SCHNEIDER, T. M., GIBSON, J. F. & BURKE, J. 2010*a* Snakes and ladders: Localised solutions of plane Couette flow. *Phys. Rev. Lett.* **104**, 104501.
- SCHNEIDER, T. M., MARINC, D. & ECKHARDT, B. 2010*b* localised edge states nucleate turbulence in extended plane Couette cells. *J. Fluid Mech.* **646**, 441.
- SCHUMACHER, J. & ECKHARDT, B. 2001 Evolution of turbulent spots in a parallel shear flow. *Phys. Rev. E* **63**, 046307.
- SKUFCA, J., YORKE, J. & ECKHARDT, B. 2006 Edge of chaos in a parallel shear flow. *Phys. Rev. Lett.* **96**, 174101.
- TOH, S. & ITANO, T. 2003 A periodic-like solution in channel flow. *J. Fluid Mech.* **481**, 67–76.
- TUCKERMAN, L., KREILOS, T., SCHROBSDORFF, H., SCHNEIDER, T.M. & GIBSON, J. F. 2014 Turbulent-laminar patterns in plane Poiseuille flow. *arXiv1312.6783*
- VISWANATH, D. 2007 Recurrent motions within plane Couette turbulence. *J. Fluid Mech.* **580**, 339.
- WALEFFE, F. 1998 Three-dimensional coherent states in plane shear flows. *Phys. Rev. Lett.* **81**, 4140.
- WALEFFE, F. 2003 Homotopy of exact coherent structures in plane shear flows. *Phys. Fluids* **15**, 1517.
- WANG, J., GIBSON, J. F. & WALEFFE, F. 2007 Lower branch coherent states in shear flows: Transition and control. *Phys. Rev. Lett.* **98**, 204501.
- ZAMMERT, S. & ECKHARDT, B. 2014 Periodically bursting edge states in plane Poiseuille flow. *Fluid. Dyn. Res.* **46**, 041419.
- ZAMMERT, S. & ECKHARDT, B. 2014*b* A spotlike edge state in plane Poiseuille flow. *Proc. Appl. Math. Mech.* submitted.